Available online at www.sciencedirect.com

ScienceDirect

Mendeleev Commun., 2024, **34**, 656–659

Mendeleev Communications

Novel dithieno[3,2-*f*:2′,3′-*h*]quinoxaline-based polymers as hole transport materials for perovskite solar cells

Ekaterina A. Komissarova,*[a] Sergei A. Kuklin,[a,b] Alina F. Latypova,[a] Sergei L. Nikitenko,[a] Victoria V. Ozerova,[a] Maria N. Kevreva,[a] Nikita A. Emelianov,[a] Lyubov A. Frolova[a] and Pavel A. Troshin[c,a]

[a] *Federal Research Center of Problems of Chemical Physics and Medicinal Chemistry, Russian Academy of Sciences, 142432 Chernogolovka, Moscow Region, Russian Federation. E-mail: ekaterina.komva@inbox.ru*
[b] *A. N. Nesmeyanov Institute of Organoelement Compounds, Russian Academy of Sciences, 119334 Moscow, Russian Federation*
[c] *Zhengzhou Research Institute of HIT, Jinshui District, 450003 Zhengzhou, China*

DOI: 10.1016/j.mencom.2024.09.010

Two novel conjugated polymers comprised of 2,3-R_2-dithieno[3,2-*f*:2′,3′-*h*]quinoxaline, where R is 3′-(octyloxy)-phenyl (P1) or 2′-(2-ethylhexyl)thiophen-4′-yl (P2), and 2,1,3-benzothiadiazole have been synthesized using the Stille cross-coupling reaction. The synthesized polymers were investigated as hole transport layer (HTL) materials in perovskite solar cells. Polymer P2 as an HTL material provided improved short-circuit current and open-circuit voltage and, correspondingly, enhanced power conversion efficiency of perovskite solar cells compared to that of polymer P1.

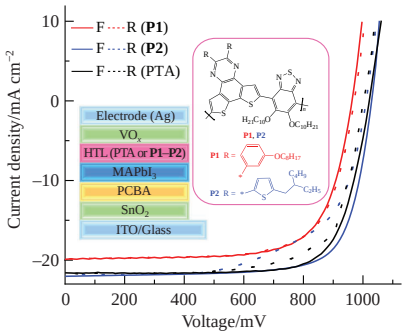

Keywords: dithieno[3,2-*f*:2′,3′-*h*]quinoxaline, 2,1,3-benzothiadiazole, Stille cross-coupling, hole transport materials, perovskite solar cells, PSCs.

Organic π-conjugated polymers represent a promising class of materials for advanced organic and hybrid photovoltaic devices, in particular, solar cells. The main advantages of polymeric materials include the ability of tuning their optical and electronic properties, high chemical and thermal stability, efficient light absorption, and high solubility. Organic π-conjugated polymers are being actively used as promising hole transport layer (HTL) materials for efficient and stable perovskite solar cells (PSCs) due to tailored frontier orbital energies, high carrier mobilities, and excellent solubility enabling their solution processing.[1–4] Recently, an impressive power conversion efficiency (PCE) of 23.1% was reported for PSCs using a dopant-free bithiopheneimide-based polymeric HTL,[5] which significantly narrows the efficiency gap between PSCs and major inorganic photovoltaic technologies using crystalline silicon or metal chalcogenides.[6]

The design and synthesis of organic conjugated polymers is one of the most important tasks for developing high-performance photovoltaic devices. The donor–acceptor (D–A) strategy is a popular approach to the preparation of π-conjugated polymers involving the incorporation of alternating electron-donating and electron-withdrawing moieties.[7–12] Various thiophene derivatives such as benzodithiophene, dithieno[3,2-*f*:2',3'-*h*]quinoxaline or thieno[3,2-*b*]thiophene are mainly used as donor moieties for the development of efficient D–A conjugated polymers because, on the one hand, they provide an optimal combination of physicochemical and optoelectronic properties.[13–15] On the other hand, 2,1,3-benzothiadiazole is a widely used acceptor moiety, since it is characterized by easy synthesis, excellent photochemical and oxidative stability, and optimal frontier energy levels.[16–18] Nevertheless, despite the progress in using conjugated polymers as HTLs for PSCs, these materials usually have sophisticated molecular structures comprised of multiple building blocks usually requiring multistep synthesis, which consequently complicates their future practical application. In this regard, a simpler and more rational design of new polymeric materials becomes relevant.

In this work we have used a relatively simple synthetic approach to prepare two novel copolymers that have been systematically explored and applied in PSCs with the n–i–p architecture. To synthesize conjugated polymers, we used the Stille polycondensation reaction, which is an efficient method enabling high selectivity and versatility. This approach is tolerant towards most highly functionalized molecules to form C–C bonds as a result of coupling between halides and organostannanes.[19,20] First, two novel monomers **M1** and **M2** based on dithieno-[3,2-*f*:2′,3′-*h*]quinoxaline with two terminal trimethylstannyl groups were synthesized in high yields. Monomer **M1** contains 3′-(octyloxy)phenyl units in positions 2 and 3 of the quinoxaline fragment, and monomer **M2** contains 2′-(2-ethylhexyl)thiophen-4′-yl fragments. The synthesis of monomers **M1** and **M2** was carried out according to known methods,[21–24] as presented in Scheme S1 in Online Supplementary Materials. 4,7-Dibromo-5,6-bis(decyloxy)benzo[*c*][1,2,5]thiadiazole **M3** used as the electron acceptor unit was synthesized in a 90% yield, and its synthesis is also shown in Scheme S1. Polymers **P1** and **P2** were synthesized *via* the palladium-catalyzed Stille cross-coupling of **M1** or **M2** with **M3** as shown in Scheme 1.

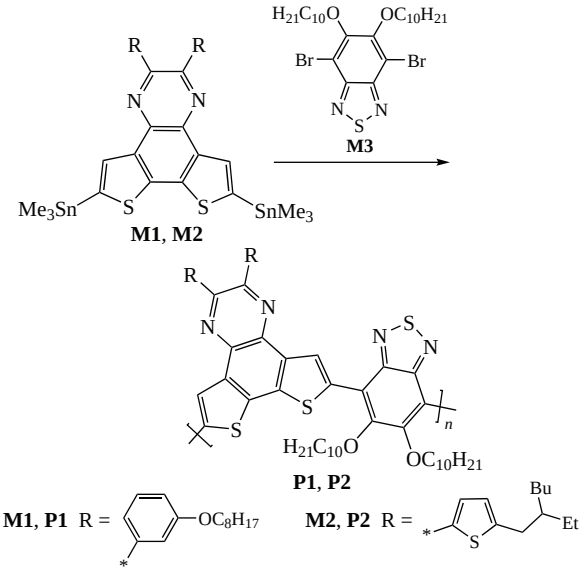

Scheme 1 *Reagents and conditions*: $Pd_2(dba)_3$ (4 mol%), (o-$MeC_6H_4)_3P$ (20 mol%), toluene, Ar, reflux, 5 h.

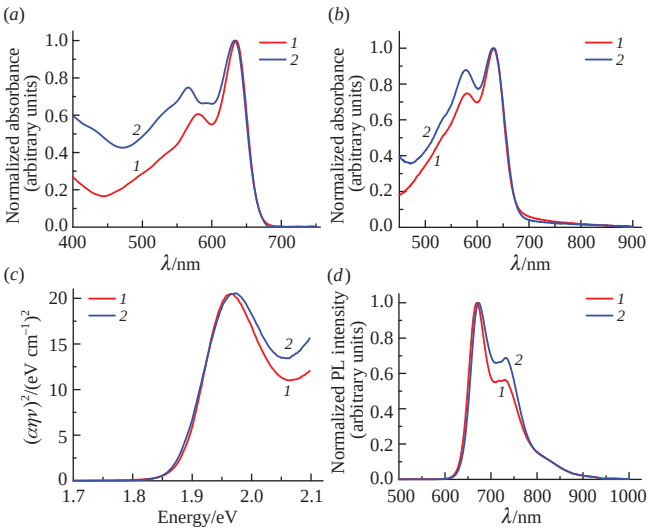

Figure 1 Absorption spectra of **P1** and **P2** in (*a*) chlorobenzene solutions and (*b*) thin films; (*c*) Tauc plots for thin films of **P1** and **P2**; (*d*) photoluminescence spectra of **P1** and **P2** in thin films.

Dynamic gel permeation chromatography (GPC) was used to monitor the polycondensation process during the synthesis of the target polymers. Crude polymers were purified from low molecular weight impurities by Soxhlet extraction using the following set of solvents: acetone, heptane, dichloromethane, and chlorobenzene. After extraction the polymer fractions were collected and concentrated under vacuum, and then the polymers were precipitated with acetone. The relative molecular weight characteristics of **P1** and **P2** analyzed by GPC are presented in Table 1.

Thermal properties of polymers **P1** and **P2** were explored using thermal gravimetry analysis (TGA). The both materials showed high thermal stability with decomposition temperatures (T_d) corresponding to 5% mass loss at 324 °C (Online Supplementary Materials, Figure S8). The optical properties of the prepared polymers **P1** and **P2** were studied in solutions and thin films using UV–VIS spectroscopy [Figure 1(*a*)–(*c*)]. Polymers **P1** and **P2** (differing in block R) demonstrated similar optical properties in chlorobenzene solutions with absorption maxima at 580, 635 and 580, 632 nm, respectively. The absorption bands in the 580–630 nm range are associated with the intramolecular charge transfer between the donor and acceptor fragments [Figure 1(*a*)]. A similar pattern is observed in the absorption spectra of **P1** and **P2** polymer thin films (see Table 1). In addition, the absorption spectra of polymers **P1** and **P2** in solutions and films are almost identical, suggesting a significant aggregation of the macromolecules even in solution at room temperature. The optical bandgaps (E_g^{opt}) for polymers **P1** and **P2** were estimated from Tauc plots. The bandgap values for both polymers are similar [see Table 1, Figure 1(*c*)]. The photoluminescence band maxima of polymers **P1** and **P2** are located at *ca*. 670 nm or 1.85 eV, which is close to the band gaps of these materials [see Table 1, Figure 1(*d*)]. In addition, the peak in the photoluminescence (PL) spectra of polymers **P1** and **P2** at ~730 nm suggests the presence of some well-organized fractions featuring stronger electronic interactions of the macromolecules.

The electrochemical properties of **P1** and **P2** were investigated using cyclic voltammetry (CV), and the CV curves are shown in Figure S9 (see Online Supplementary Materials). The HOMO and LUMO energies were estimated using a standard approach: $E_{HOMO} = -[E_{ox}(\text{onset } vs.\ Fc^+/Fc) + 4.8]/eV$[25] and $E_{LUMO} = E_g + E_{HOMO}/eV$. The corresponding numeric data are summarized in Table 1. The HOMO energy of polymer **P1** with 3′-(octyloxy)phenyl units was estimated as −5.36 eV, while for polymer **P2** bearing 2′-(2-ethylhexyl)thiophen-4′-yl blocks the HOMO energy was estimated as −5.22 eV. The obtained data show that the HOMO energy of polymer **P1** better matches the top of the valence band of the perovskite absorber (*ca.* −5.43 eV for methylammonium lead iodide $MAPbI_3$),[26] than that of polymer **P2**, which may be the main prerequisite for the efficient extraction of holes in HTLs and their transport to the corresponding electrode.[27,28] The LUMO energy of **P1** (−3.48 eV) is also lower than that of **P2** (−3.35 eV).

The photovoltaic performance of **P1** and **P2** as the dopant-free HTL materials has been investigated in PSCs assembled with the following device architecture: ITO/SnO_2/PCBA/$MAPbI_3$/HTL/VO_x/Ag, as shown in Figure 2(*a*). To passivate surface defects on the SnO_2 layer, we deposited a layer of phenyl-C_{61}-butyric acid [PCBA, Figure 2(*b*)]. Poly(bis(4-phenyl)(4′-methylphenyl)amine) known as PTA was used as a reference HTL material [Figure 2(*b*)]. Figures 2(*c*)–(*d*) show the current–voltage characteristics of the champion devices with **P1** and **P2** as HTLs and their external quantum efficiency (EQE) spectra, whereas the device parameters are given in Table 2.

Table 1 Physicochemical and optoelectronic properties of **P1** and **P2**.

Polymer	M_w[a]/kDa	M_w/M_n[b]	T_d[c]/°C	$\lambda_{max}^{sol}(\lambda_{max}^{film})$/nm[d]	E_g^{opt}/eV[e]	λ_{PLmax}[f]/nm	$E_{onset}^{ox.}$[g]/V *vs.* Fc^+/Fc	HOMO (LUMO)[h]/eV
P1	153	1.32	324	580, 635 (580, 632)	1.88	669, 729	0.56	−5.36 (−3.48)
P2	55	1.71	324	566, 632 (578, 630)	1.87	673, 732	0.42	−5.22 (−3.35)

[a] Weight-average molecular weight. [b] Polydispersity index. [c] Temperature corresponding to 5% mass loss. [d] Absorption maxima of polymers in solution (thin film). [e] Optical energy bandgap estimated using Tauc plots of thin film absorption spectra. [f] Photoluminescence maxima of polymer thin films. [g] Oxidation potential. [h] HOMO energy estimated from CV measurements, and LUMO energy estimated as E_g^{opt} + HOMO.

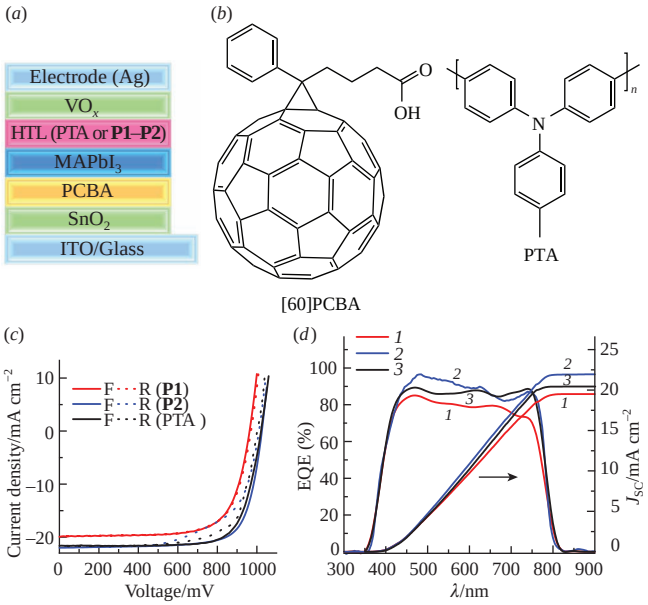

Figure 2 (*a*) Configuration of PSC; (*b*) structures of PCBA and PTA; (*c*) *J*–*V* characteristics and (*d*) EQE spectra and short-circuit current density of PSCs using **P1** and **P2** as HTL materials. Scan direction: F – forward; R – reverse.

Table 2 Characteristics of n–i–p PSCs fabricated using polymers **P1** and **P2** and PTA as HTLs.

HTL	Scan direction	V_{OC}[a]/V	J_{SC}[b]/mA cm^{-2}	FF[c] (%)	PCE[d] (%)
P1	Forward	0.963	19.9	71	13.7
	Reverse	0.971	19.7	71	13.7
P2	Forward	1.026	22.0	75	16.9
	Reverse	1.011	21.8	62	13.7
PTA	Forward	1.023	21.8	74	16.6
	Reverse	1.014	21.6	73	15.8

[a]Open-circuit voltage. [b]Short-circuit current density. [c]Fill factor. [d]Power conversion efficiency.

PSCs with **P2** as a HTL showed a PCE of 16.9%, while the cells with polymer **P1** showed a PCE of 13.7%. The devices with **P2** showed improved open-circuit voltage (V_{OC}) and short-circuit current density (J_{SC}) characteristics of 1.026 V and 22.0 mA cm^{-2}, respectively, compared to the devices with **P1**, whose respective values were 0.963 V and 19.9 mA cm^{-2}. The devices with polymer **P2** show similar characteristics to those of PSCs with PTA, which is a positive result.

In order to better understand the factors controlling the photovoltaic performance of PSCs containing **P1** and **P2**, we investigated the morphology and uniformity of polymer films deposited on the top of a perovskite absorber layer using atomic force microscopy (AFM) and scattered scanning infrared near-field optical microscopy (IR s-SNOM). A detailed description of this method was published elsewhere.[29]

Figure S10 (see Online Supplementary Materials) shows the IR s-SNOM mapping images for the perovskite films coated with **P1** and **P2** and PTA. The data for $MAPbI_3$/**P1** and $MAPbI_3$/**P2** samples reveal the presence of point defects being more visible in the case of the $MAPbI_3$/**P2** system. A similar pattern is observed when using conventional IR scanning microscopy for $MAPbI_3$/**P1** and $MAPbI_3$/**P2** samples over a larger area (Figure S12). Additionally, the IR s-SNOM images for $MAPbI_3$/**P1** and $MAPbI_3$/**P2** samples exhibit weak contrast, which is likely due to the peculiarities of surface topography of the perovskite layer as revealed in the AFM images (Figure S10, left column). Figure S10 (center column) illustrates that the polymer films are thinner at the top of the perovskite grains, which makes visible a weak signal corresponding to the perovskite sublayer. Probably, the nonuniformity of polymeric HTLs degrades the photovoltaic performance of the PSCs with **P1** and **P2**. Thus, the optimization of the surface morphology of the polymer films deposited on the perovskite absorber layer may be one of the ways to enhance the photovoltaic performance of PSCs using **P1** and **P2** as HTLs.

In conclusion, we have synthesized two new monomers based on 2,3-disubstituted-dithieno[3,2-*f*:2′,3′-*h*]quinoxaline with two terminal trimethylstannyl groups. These monomers were used to synthesize conjugated polymers *via* the Stille reaction with 4,7-dibromo-5,6-bis(decyloxy)benzo[*c*][1,2,5]thiadiazole. The resulting polymers were investigated and applied as HTL materials in PSCs. Polymer **P2** based on 2,3-di(2′-(2-ethylhexyl)thiophen-4′-yl)dithieno[3,2-*f*:2′,3′-*h*]quinoxaline and 2,1,3-benzothiadiazole enabled a higher power conversion efficiency of PSCs. The optimization of the surface morphology of the polymer films deposited on the perovskite absorber layer may further increase the PCE of photovoltaic devices. The obtained results demonstrate a good potential of this type of derivatives to be applied as structurally simple and inexpensive hole transport materials for PSCs.

This work was supported by the Russian Science Foundation (grant no. 23-73-01196).

Online Supplementary Materials

Supplementary data associated with this article can be found in the online version at doi: 10.1016/j.mencom.2024.09.010.

References

1 X. Sun, X. Yu and Z. Li, *ACS Appl. Energy Mater.*, 2020, **3**, 10282.
2 C. Sun, C. Zhu, L. Meng and Y. Li, *Adv. Mater.*, 2022, **34**, 2104161.
3 G. Xie, J. Chen, H. Li, J. Yu, H. Yin, Z. Wang, Y. Huang, C. Feng, Y. Pan, A. Liang and Y. Chen, *Chin. J. Chem.*, 2023, **41**, 3133.
4 C. Zhang, K. Wei, J. Hu, X. Cai, G. Du, J. Deng, Z. Luo, X. Zhang, Y. Wang, L. Yang and J. Zhang, *Mater. Today*, 2023, **67**, 518.
5 Y. Bai, Z. Zhou, Q. Xue, C. Liu, N. Li, H. Tang, J. Zhang, X. Xia, J. Zhang, X. Lu, C. J. Brabec and F. Huang, *Adv. Mater*., 2022, **34**, 2110587.
6 G. Ren, W. Han, Y. Deng, W. Wu, Z. Li, J. Guo, H. Bao, C. Liu and W. Guo, *J. Mater. Chem. A*, 2021, **9**, 4589.
7 C. Liu, L. Shao, S. Chen, Z. Hu, H. Cai and F. Huang, *Prog. Polym. Sci*., 2023, **143**, 101711.
8 C. S. Sarap, Y. Singh, J. M. Lane and N. Rai, *Sci. Rep*., 2023, **13**, 21587.
9 A. G. S. Al-Azzawi, S. B. Aziz, E. M. A. Dannoun, A. Iraqi, M. M. Nofal, A. R. Murad and A. M. Hussein, *Polymers*, 2023, **15**, 164.
10 K. Mahesh, S. Karpagam and K. Pandian, *Top. Curr. Chem*., 2019, **377**, 12.
11 P. M. Kuznetsov, I. E. Kuznetsov, I. V. Klimovich, P. A. Troshin and A. V. Akkuratov, *Mendeleev Commun.*, 2021, **31**, 30.
12 A. F. Latypova, A. V. Maskaev, L. G. Gutsev, N. A. Emelianov, I. E. Kuznetsov, P. M. Kuznetsov, S. L. Nikitenko, Y. V. Baskakova, A. V. Akkuratov, E. A. Komissarova, L. A. Frolova, S. M. Aldoshin and P. A. Troshin, *Mater. Today Chem*., 2022, **26**, 101218.
13 J. W. Jung, J. W. Jo, E. H. Jung and W. H. Jo, *Org. Electron*., 2016, **31**, 149.
14 F. Zhang, Z. Yao, Y. Guo, Y. Li, J. Bergstrand, C. J. Brett, B. Cai, A. Hajian, Y. Guo, X. Yang, J. M. Gardner, J. Widengren, S. V. Roth, L. Kloo and L. Sun, *J. Am. Chem. Soc*., 2019, **141**, 19700.
15 S. A. Kuklin, S. V. Safronov, O. Yu. Fedorovskii, E. A. Khakina, L. V. Kulik, D. E. Utkin, L. A. Frolova, P. A. Troshin and A. R. Khokhlov, *Mendeleev Commun.*, 2023, **33**, 306.
16 P. Cong, Z. Wang, Y. Geng, Y. Meng, C. Meng, L. Chen, A. Tang and E. Zhou, *Nano Energy*, 2023, **105**, 108017.
17 Y. Zhang, J. Song, J. Qu, P.-C. Qian and W.-Y. Wong, *Sci. China: Chem.*, 2021, **64**, 341.
18 M. L. Keshtov, A. R. Khokhlov, S. A. Kuklin, S. A. Osipov, N. A. Radychev, M. I. Buzin and G. D. Sharma, *Org. Electron.*, 2017, **41**, 1.
19 N. Miyaura and A. Suzuki, *Chem. Rev*., 1995, **95**, 2457.

20 P. Espinet and A. M. Echavarren, *Angew. Chem., Int. Ed*., 2004, **43**, 4704.
21 L. Marin, L. Lutsen, D. Vanderzande and W. Maes, *Org. Biomol. Chem*., 2013, **11**, 5866.
22 F. A. Arroyave, C. A. Richard and J. R. Reynolds, *Org. Lett*., 2012, **14**, 6138.
23 J. Pina, A. Eckert, U. Scherf, A. M. Galvão and J. S. Seixas de Melo, *Mater. Chem. Front*., 2018, **2**, 149.
24 M. L. Keshtov, S. A. Kuklin, I. O. Konstantinov, I. E. Ostapov, Zh. Xie, E. N. Koukaras, R. Suthar and G. D. Sharma, *Sol. Energy*, 2020, **205**, 211.
25 C. M. Cardona, W. Li, A. E. Kaifer, D. Stockdale and G. C. Bazan, *Adv. Mater*., 2011, **23**, 2367.
26 Q. Guo, H. Liu, Z. Shi, F. Wang, E. Zhou, X. Bian, B. Zhang, A. Alsaedi, T. Hayat and Z. Tan, *Nanoscale*, 2018, **10**, 3245.
27 X. Yin, Z. Song, Z. Li and W. Tang, *Energy Environ. Sci*., 2020, **13**, 4057.
28 P. Schulz, E. Edri, S. Kirmayer, G. Hodes, D. Cahen and A. Kahn, *Energy Environ. Sci*., 2014, **7**, 1377.
29 A. F. Latypova, N. A. Emelianov, D. O. Balakirev, P. K. Sukhorukova, N. K. Kalinichenko, P. M. Kuznetsov, Y. N. Luponosov, S. M. Aldoshin, S. A. Ponomarenko, P. A. Troshin and L. A. Frolova, *ACS Appl. Energy Mater*., 2022, **5**, 5395.

Received: 4th April 2024; Com. 24/7446